*Fifth International Conference on CFD in the Process Industries*
*CSIRO, Melbourne, Australia*
*13-15 December 2006*

# TIME DEPENDENT ELECTRIC, MAGNETIC AND HYDRODYNAMIC INTERACTION IN ALUMINIUM ELECTROLYSIS CELLS

**Valdis BOJAREVICS and Koulis PERICLEOUS**

University of Greenwich, CMS, Park Row, London, SE10 9LS, UK

## ABSTRACT

The waves in commercial cells for electrolytic aluminium production originate at the interface between the liquid aluminium and electrolyte, but their effect can spread into the surrounding busbar network as electric current perturbation, and the total magnetic field acquires a time dependent component. The presented model for the wave development accounts for the nonuniform electric current distribution at the cathode and the whole network of the surrounding busbars. The magnetic field is computed for the continuous current in the fluid zones, all busbars and the ferromagnetic construction elements. When the electric current and the associated magnetic field are computed according to the actual electrical circuit and updated for all times, the instability growth rate is significantly affected. The presented numerical model for the wave and electromagnetic interaction demonstrates how different physical coupling factors are affecting the wave development in the electrolysis cells. These small amplitude self-sustained interface oscillations are damped in the presence of intense turbulent viscosity created by the horizontal circulation velocity field. Additionally, the horizontal circulation vortices create a pressure gradient contributing to the deformation of the interface. Instructive examples for the 500 kA demonstration cell are presented.

## NOMENCLATURE

$A$ wave amplitude
$\mathbf{B}$ magnetic field
E nondimensional electromagnetic interaction parameter
$\mathbf{f}$ electromagnetic force
$\mathbf{H}$ magnetic field intensity
$H=H_1$ typical depth (aluminium)
$\bar{H} = H/(L\delta)$ nondimensional depth
$I$ total electric current
$\mathbf{J}$ electric current density
$L=L_y$ characteristic length
$\mathbf{M}$ magnetization
$p$ pressure
Re Reynolds number
$\mathbf{u}$ velocity
$\hat{\mathbf{u}}$ depth averaged
$\varepsilon$ amplitude parameter
$\delta$ depth parameter
$\zeta$ nondimensional interface
$\mu=C_f|\hat{\mathbf{u}}|$ bottom friction coefficient
$\rho$ density
$\sigma$ electrical conductivity
$\nu$ kinematic viscosity

## INTRODUCTION

The interface stability problem for aluminium electrolysis cells is of great practical importance due to significant electrical energy losses, disruptions in the technology and increased environmental pollution rate. The electric current penetrating the electrolytic cells, together with the associated magnetic field, are intricately involved in the oscillation process at the interface between liquid aluminium and electrolyte. This interaction results in the observed wave frequencies being shifted from the purely hydrodynamic ones (Von Kaenel and Antille, 1996). The first attempts of the stability analysis date back to 70s (Urata 1976, Sele 1977). The multiple mode interaction was mathematically shown by Sneyd and Wang, 1994. Moreau and Evans, 1984, introduced the linear friction model for the wave motion and the horizontal circulation, and it was widely used afterwards in numerical studies. Actually, the linear friction is a simplification of the more general nonlinear bottom friction term appearing in the shallow water models, see for example Rastogi and Rodi 1978. The systematic perturbation theory for the fluid dynamics and electric current problems, permitting to reduce the three-dimensional problem of the aluminium cell to a two-dimensional shallow layer problem was developed by Bojarevics and Romerio 1994. This work mathematically proved the wave oscillation frequency shift due to the magnetic interaction and the possibility of a resonant growth when two independent frequencies are moved to coincide. The wave model has been extended to the weakly nonlinear case using the Boussinesq formulation including the linear dispersion terms (Bojarevics 1998). The intense turbulence generated by the horizontal circulation velocity is essential in order to explain the small amplitude self-sustained oscillations observed in real cells, known as 'MHD noise'. A generalisation of the non-linear wave equations accounting for the turbulent horizontal circulation flow in the two fluid layers is just a first step. The second vital step for the fully coupled real cell problem requires the time dependent, extended electromagnetic field simulation including the fluid layers, the whole bus bar circuit and the ferromagnetic effects. An instructive analysis of the results achieved with such a numerical model was started recently (Bojarevics and Pericleous, 2006). The present paper extends the study to the cases of time dependent magnetic field effects, new stable bus bar arrangement for the 500 kA cells, and the turbulent horizontal circulation coupling.

## MODEL DESCRIPTION

### Shallow Water Approximation

Electrolytic cells are arranged in series of long rows via a complex network of current-carrying bus bars. An example of the 500 kA cells modelled in the paper is shown in Figure 1. The liquid electrolyte layer beneath the anode blocks is a relatively poor electrical conductor of a small depth ($H_2$=0.04-0.05 m) if compared to its horizontal extension ($L_y$=3-4 m width, $L_x$=10-20 m length). The electrolyte density ($\rho_1$ = 2100 kg/m$^3$) is slightly less than the liquid aluminium ($\rho_2$ = 2300 kg/m$^3$) of the bottom layer of typical depth $H_1$=15–30 cm. The "shallow water" approximation assumes that the horizontal dimensions are much larger than the typical depth $H$ for each of the layers and, in addition to this, the interface wave amplitude $A$ is assumed to be small relative to the depth $H$. Therefore there are two small parameters of the problem: the nondimensional depth $\delta = H/L$ and the amplitude $\varepsilon = A/H$. The more detailed derivation of the Boussinesq equations for the wave motion and the coupled horizontal circulation velocities are given in previous publications (see Bojarevics and Pericleous, 2006 and the references therein). The resulting fluid dynamic equations become two-dimensional after the depth averaging procedure is applied to the horizontal momentum equations. The equations for the combined horizontal velocity (horizontal circulation $\mathbf{u}_0$, plus ε-order $\hat{\mathbf{u}}_\varepsilon$ wave motion) are

$$\hat{\mathbf{u}} = (\bar{H}_i - \bar{H}_o)^{-1}\int \mathbf{u}\, d\bar{z} = \mathbf{u}_0 + \varepsilon\hat{\mathbf{u}}_\varepsilon \qquad (1)$$

$$\rho(\partial_t \hat{u}_j + \hat{u}_k \partial_k \hat{u}_j) = -\partial_j p(\bar{H}_0) - \varepsilon\partial_j \varsigma - \mu\hat{u}_j + \mathrm{Re}^{-1}\,\partial_k \nu_e \partial_k \hat{u}_{0j} + E\,\hat{f}_j - \tfrac{1}{2}\delta E \bar{H}_i \partial_j \hat{f}_z\,, \qquad (2)$$

where the continuity of the pressure at the interface is satisfied by introducing the pressure $p(\bar{H}_0)$ at the common interface. The summation convention is assumed over the repeating indexes $k$ (1 or 2, respectively for $x$, $y$ coordinates). The horizontal coordinates are made nondimensional by the horizontal length scale $L$ and, according to the small depth assumption, the nondimensional interface deformation of small amplitude is represented as

$$\bar{H}_0 = H_0/(L\delta) = \varepsilon\ \varsigma(x,y,t)\,. \qquad (3)$$

The nondimensional variables are introduced using the following typical scales: the typical gravitational wave velocity is scaled as $u_0 = \sqrt{gH}$, $L/\sqrt{gH}$ for time $t$, $\rho_1 u_0^2$ for pressure $p$, $IB_0/L^2$ for the electromagnetic force $\mathbf{f}$ ($B_0$ is typical magnetic field magnitude and $I$ the total electric current), the relative density $\rho = \rho_i / \rho_1$. The nondimensional parameters are the Reynolds number Re and the electromagnetic interaction parameter E:

$$\mathrm{Re} = Lu_0/\nu\,,$$

$$\mathrm{E} = (IB_o/L^2)/(\rho_1 u_0^2/L) = IB_o/(L^2\rho_1 g\delta)\,.$$

The effective turbulent viscosity $\nu_e(x,y,t)$ is computed according to the depth averaged versions of empirical turbulence models. For our simulations we used a version of $k$-$\omega$ two equation model previously validated for various recirculating MHD flows (Bojarevics et al. 2004).

The nonlinear friction at the top and bottom of the fluid layers in (2) is defined similarly to general shallow water models (Rastogi and Rodi, 1978):

$$\mu\hat{u}_j = C_f|\hat{\mathbf{u}}|\hat{u}_j = \mathbf{Re}^{-1}\delta^{-2}(\bar{H}_i - \bar{H}_o)^{-1}\int \partial_{\bar{z}}\nu_e\partial_{\bar{z}}u_j\, d\bar{z}\,. \qquad (4)$$

The equations of momentum (2) and the depth averaged continuity

$$\varepsilon\partial_t\varsigma = \partial_j[(\bar{H}_i - \varepsilon\varsigma)\hat{u}_j]\,, \qquad (5)$$

for the two fluid layers can be combined into a single nonlinear wave equation for the interface ζ(x,y,t) by taking the time derivative of (4) and the horizontal divergence of (2). Then the difference between the resulting equations for the two layers permits to eliminate the common pressure at the interface $p(\bar{H}_0)$, yielding:

$$\begin{aligned}&\varepsilon\left\langle\rho/\bar{H}\right\rangle\partial_{tt}\varsigma + \varepsilon\left\langle\mu\rho/\bar{H}\right\rangle\partial_t\varsigma + \varepsilon\left\langle\rho\right\rangle\partial_{jj}\varsigma = \\ &E\left\langle\partial_j\hat{f}_j\right\rangle - \delta E\left\langle\tfrac{1}{2}\bar{H}\partial_{jj}\hat{f}_z\right\rangle \\ &-\varepsilon\left\langle\rho/\bar{H}\partial_{tj}(\varsigma u_{jo}) + \mu\rho/\bar{H}\partial_j(\varsigma u_{jo})\right\rangle - \left\langle\rho\partial_j(\hat{u}_k\partial_k\hat{u}_j)\right\rangle\end{aligned} \qquad (6)$$

where $\langle F\rangle = F_1 - F_2$ denotes difference of the respective variable in the two layers. The previous linear stability model (Bojarevics and Romerio, 1994) can be recovered from (6) by excluding the nonlinear and the dispersion terms. However, the nonlinear equation (6) extends the wave description to the weakly nonlinear case, where, for instance, a solitary wave with the electromagnetic interaction can be described. The horizontal circulation velocities, driven by the rotational part of the electromagnetic force, can be calculated by solving equation (2) in the two layers. The numerically efficient procedure consists of taking first the curl of the equation (2), then to rewrite it for the two dimensional horizontal flow stream function. The solution of the resulting 4th order equation for the stream function is sought in combination with the 2-equation turbulence model for the effective viscosity.

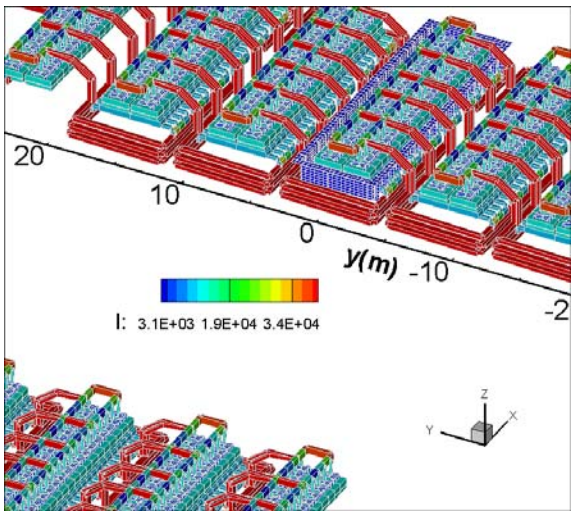


**Figure 1**: The model busbar current distribution for 500 kA cells in two potlines and the steel shell at the test cell.

### MHD Computational Model

The design of bus network for high amperage reduction cells requires optimizing the magnetic field within the cell and the electric current distribution both within the cell and the bus bars. Since the magnetohydrodynamic driving force is **j**x**B**, the electric current distribution, particularly the horizontal components, are equally important to the magnetic field optimization. Physical and engineering considerations suggest that both problems are mutually interconnected and should be solved interactively. It means that the computer program could use the same data input to compute the electric current, voltages, temperatures in the bus network, the magnetic field, the current distribution within the cell with waving metal interface, then finally iterate back to account for the spatially and temporally variable cell interpolar distance and the effect on the current distribution in the supplying bus network. This affects also the magnetic field, the metal pad waves, velocities, and the neighbour cells which are interconnected to the particular test cell (see Figure 1 for the model representation of the 500 kA cells).

#### *Electric Current Distribution*

The electric current distribution is calculated by coupling the electric current in the fluid zone to the resistance network representing the elements of individual anodes and cathode collector bars, as well as the whole bus-bar circuit between two adjacent cells. The electric current in the fluid zones is computed from the continuous media equations governing the DC current (which can change in time with the waves and anode burnout process):

$$\mathbf{j} = -\sigma\nabla\varphi + \sigma\mathbf{v}\times\mathbf{B}, \tag{7}$$

where the fluid flow induced currents are accounted for only in the highly conducting liquid aluminium. The electric potential in the fluid is governed by the equation:

$$\nabla^2\varphi = \nabla\cdot(\mathbf{v}\times\mathbf{B}), \tag{8}$$

and the boundary conditions of zero current at the insulating walls, given current distribution $\mathbf{j_a}$ at anodes, $\mathbf{j_c}$ at cathode carbon. $\mathbf{j_a}$ and $\mathbf{j_c}$ are obtained from the linear element resistivity network solution, which in turn is coupled to the computed potential distribution from the equation (8). At the interface between the liquid metal and the electrolyte the continuity of the potential and the electric current normal component must be satisfied. Since the depths of the liquid layers are extremely small if compared to their horizontal extension, the shallow layer approximation is very efficient to solve this 3-dimensional problem. The solution, for instance in the aluminium layer, can be obtained from the following equation:

$$\begin{aligned} &j_{za}(x,y,t) - j_{zc}(x,y,t) = \\ &\sigma_{Al}\partial_k((H_{Al}(x,y,t) - H_c)\partial_k\varphi), \end{aligned} \tag{9}$$

where the aluminium pad interface $H_{Al}$ (x,y,t) is variable, and the current distribution at the top and the bottom depend on the iterative solution from the linear element network of the bus bars, anodes, pins, collector bars, etc. (see Figure 1 showing the full network used in this paper).

At the beginning of the computer simulation the MHD package generates automatically a very large set of Kirchhoff equations from the relatively simple unified data input. The current distribution in the bus bar network can be described to reasonable approximation accuracy by linear resistance elements. The electric currents and voltages in such a complex, multiply connected circuit are governed by the Kirchhoff laws. For the automatic circuit analysis purpose the 'nodal' analysis is more convenient than the 'mesh' analysis. The following equation set arises for the total number of *M* nodes each of which has *N* directly connected neighbour resistances:

$$U_m \sum_{n=1}^{N} \frac{1}{R_n} - \sum_{n=1}^{N} \frac{U_n}{R_n} = I_m \ , \tag{10}$$

where $U_m$ is the potential at a node, $U_n$ - for nodes at other ends of neighbour bars, $R_n$ - resistances of neighbour bars, $I_m$ - external current entering the node. In our case total current 'I' enters the reference nodes in the liquid of the upstream cell and '-I' current leaves the nodes at the liquid metal of the downstream cell. For all other nodes the external current - right side of the equation - is zero. After finding the potentials at the nodes, the potential difference between two neighbour nodes multiplied by the connecting resistance gives the current in each resistance. A further improvement in accuracy is achieved by computing Joule heating $R_m I_m^2$ for each of the resistance elements. Knowing the Joule heating, losses to the ambient air and the connectivity of the bars, it is possible to compute the temperature of a bar. When the temperatures are calculated, the new resistances are calculated, the electric circuit equation set is solved again to iterate the whole procedure while the convergence is achieved. The convergence is easily established for bars with physically reasonable cross sections and effective heat transfer to the ambient air and to the neighbour bars. The described procedure is sufficiently flexible to permit simulation of anode changes, disconnected cathode bars, various branching of the current path between the cells, etc.

#### *Magnetic Field Distribution*

Magnetic field in an aluminium cell is created by the currents in the cell itself and from the complex bus-bar arrangement around the cell, in the neighboring cells and the return line, and by the effect of cell construction steel magnetization. The complexity of any practically usable magnetohydrodynamic (MHD) model of the cell arises from the coupling of the various physical effects: fluid dynamics, electric current distribution, magnetic field and thermal field. The MHD model presented here accounts for the time dependent coupling of the current and magnetic fields with the bath-metal interface movement.

The second step in the MHD model is to calculate the magnetic field **B**, which is necessary to determine the electromagnetic force distribution within the liquid zone, **f = j x B**. The magnetic field **B** is the sum of two contributions: $\mathbf{B} = \mathbf{B_I} + \mathbf{B_M}$ ; $\mathbf{B_I}$ is generated by currents and $\mathbf{B_M}$ by ferromagnetic steel material. The magnetic field $\mathbf{B_I}$ from the currents in the full bus-bar network is recalculated at each time step during the dynamic simulation using the Biot-Savart law. A very similar technique is used on the 3D grid within the cell fluid

layers where a special analytical technique is applied to deal with the singularity in the Biot-Savart law in order to obtain a smooth and converging solution when the field calculation position coincides to the electric current.

The calculation of the magnetic field $\mathbf{B_M}$ from steel requires much more effort. The difficulty arises because the steel parts of the cell are made of ferromagnetic material whose magnetization **M** (**H**) depends non-linearly on the local magnetic field intensity **H** in the magnetic material. The local magnetic field (induction) **B** in the ferromagnetic material is orders of magnitude higher than in the non-magnetic material, like air, liquid aluminium, electrolyte etc. Equation (11) gives the relationship between magnetic induction, magnetization and magnetic field intensity.

$$\mathbf{B} = \mu_0(\mathbf{M} + \mathbf{H}) \tag{11}$$

where $\mu_0$ is the permeability of vacuum, equal to $4\pi \times 10^{-7}$ (H/m). In the magnetic material the unknown magnetic field intensity **H** is related to the magnetization **M** (**H**) by the material properties of a particular material (depending also on the temperature, carbon content in steel, previous magnetization). In order to find the unknown magnetic field intensity, we need to solve the integral equation:

$$\mathbf{H}(\mathbf{r}) = \mathbf{H}_I(\mathbf{r}) - \frac{1}{4\pi}\int_{V_m}\left[\frac{\mathbf{M}(\mathbf{r}')}{|\mathbf{r}-\mathbf{r}'|^3} - \frac{3(\mathbf{r}-\mathbf{r}')}{|\mathbf{r}-\mathbf{r}'|^5}(\mathbf{r}-\mathbf{r}')\cdot\mathbf{M}(\mathbf{r}')\right]dV', \tag{12}$$

where the magnetic field $H_I$ is given by the Biot-Savart law from all the external electric currents, the co-ordinate location r is for the field calculation position (observation point), the integration point position r' is in the element volume dV' running through all the ferromagnetic material in $V_m$. The iterative solution procedure for the equation (12) calculates H for the elements, then uses M (H) material property to obtain the updated magnetization. The obvious complication is due to the singularity in (12) when the integration point coincides with the observation point. This is a very important contribution to the solution and can not be simply discarded; instead the analytical singularity elimination is used to give smooth results. Once the magnetization of steel is known, the magnetic flux density $B = \mu_0 H$ for the fluid zones is calculated from the equation (12). For the magnetic field computation, the busbar network is extended to include 6 neighboring cells as shown in Figure 1. The ferromagnetic parts are divided into approximately 30000 nonlinear elements. Figure 2 shows the magnetic field distribution in the steel potshell, from which the location of the major electric bus elements can be easily recognized.

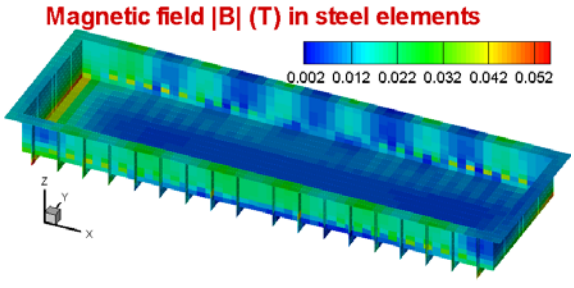


**Figure 2**: Magnetic field in the steel shell.

## TIME DEPENDENT SIMULATION RESULTS FOR 500 KA CELL

The MHD model uses a relatively coarse mesh of 64x32x2 in each fluid layer in order to be able to re-compute the electromagnetic and fluid dynamic fields time dependent distribution in a reasonable execution time. Nevertheless, the solution is sufficiently smooth because of the global pseudo-spectral approximation used for the velocity and interface discretisation, which permits much higher accuracy in comparison to finite element or finite volume approximations on the similar grid size.

The aluminium-electrolyte interface deformation makes the anode currents unequal because of the local ACD change. The model includes an option to account for the time average gradual consumption of the anode bottom to conform to the ACD change. An artificially accelerated anode burn-out is permitted in order to achieve the result in a reasonable computational time interval. The importance of this option was demonstrated in the recent study (Bojarevics and Pericleous, 2006) demonstrating a significant stabilization effect. It was activated for the following cases.

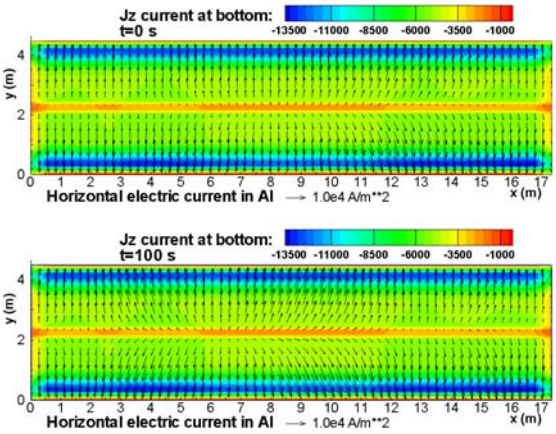


**Figure 3**: Electric current in the liquid metal at initial stage and after the interface wave development.

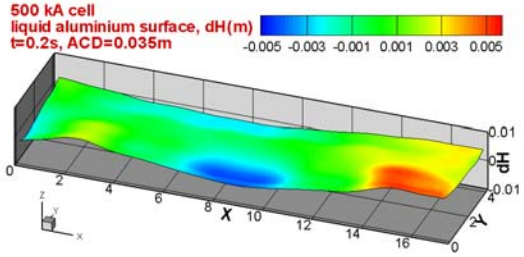


**Figure 4**: The liquid metal surface for the reduced ACD =0.035m at an initial time moment.

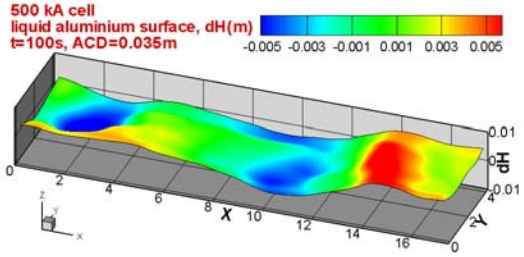


**Figure 5**: The liquid metal surface for the reduced ACD =0.035m at t=100 s.

The solution for the coupled MHD problem of the electrolysis cell demonstrates strong correlation between different fields during the wave process development. The electric current in the aluminium layer develops rather significant horizontal components because of the varying electrolyte thickness. As seen from Figure 3, the horizontal current flow is affected by the interface waving. The two corresponding time moment interface shapes are presented in the Figures 4 and 5 respectively.

The bus bar arrangement for the present study was further optimized in order to reduce the vertical magnetic field average value from about 9 Gs to 6 Gs, and to reduce the local Bz extremum magnitudes from about 32 Gs to 18 Gs. Figure 6 shows the 3 dimensional view of the magnetic field distribution at the top of the liquid metal. The magnetic field is time dependent, and it oscillates very similarly to the interface oscillation pattern as clearly demonstrated in Figure 7. Remarkably the Fourier power spectra demonstrate that exactly the same frequency oscillation is excited for the magnetic field as for the liquid metal surface. Physically the source for these variations in the **B** field are the electric currents in the liquid metal and in the nearby bus bars.

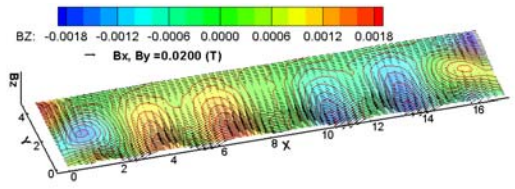


**Figure 6**: Magnetic field in the liquid metal.

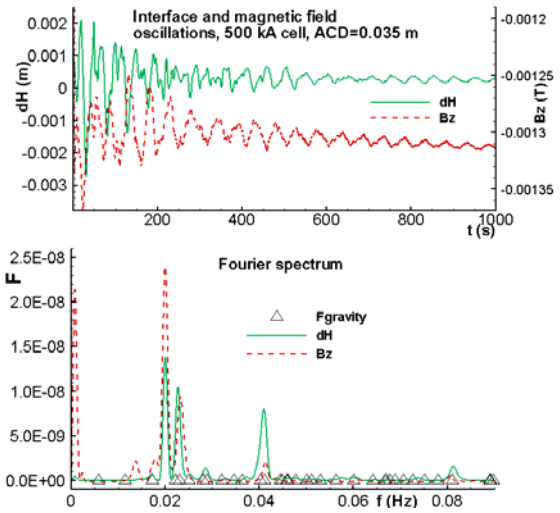


**Figure 7**: The oscillations (top) and the corresponding Fourier spectra (bottom) compared for the liquid metal surface and the magnetic field updated at all times.

The above results are presented for a slightly reduced average ACD of 0.035 m instead of the target value of 0.045 m, because a small oscillation is more visible in the former case. When the ACD is increased to 0.045 m, the cell becomes very stable when the magnetic field is updated at all times continuously. However, if we choose not to update the **B** field in time, and to keep it fixed as computed for the initial 'stationary' interface shape, then the cell becomes less stable with some oscillations as can be seen from Figure 8. The Fourier spectra peaks are also rather different. With the stationary **B** the interface oscillation exhibits one single peak, while the time dependent **B** gives significantly smaller amplitude peaks at 3 different frequencies. This indicates that the full time dependent model includes a physical parametric damping mechanism by the self adjusting magnetic field. It is worth to note that the **B** variation is just of an order of less than 1 Gauss, but the parametric damping is clearly seen for the interface effect. The corresponding interface shapes are shown in Figures 9 and 10 for the same time moments.

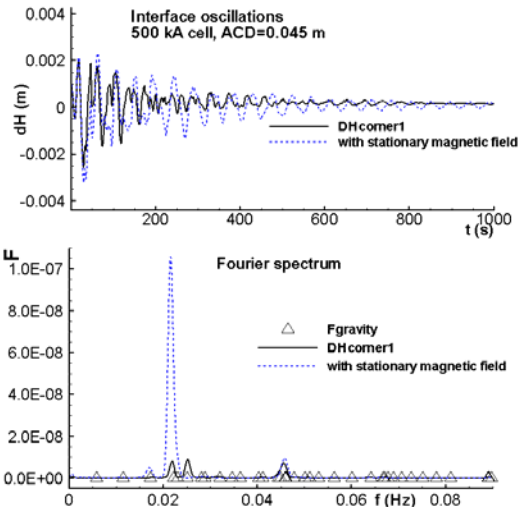


**Figure 8**: The liquid metal surface oscillations (top) and the corresponding Fourier spectra (bottom) compared when the magnetic field is either updated at all times or kept stationary as computed for the initial moment.

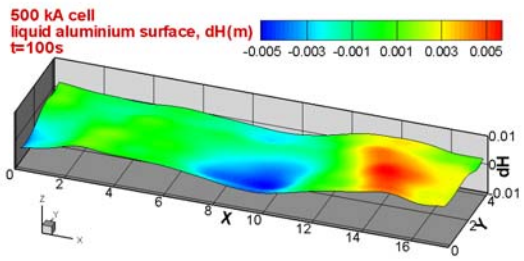


**Figure 9**: The liquid metal surface for the ACD =0.045 m at t=100 s when the magnetic field **B** is updated continuously.

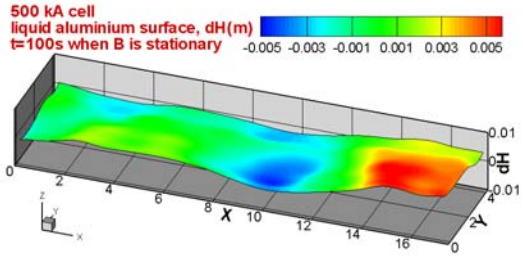


**Figure 10**: The liquid metal surface for the ACD =0.045m at t=100 s when the magnetic field **B** is kept stationary.

As noted previously, the horizontal circulation velocity distributions in the two layers have a profound effect on

the cell stability. The velocity patterns with the generated turbulent kinetic energy distributions are shown in Figures 11 and 12. The differences in the vortex centre locations and their intensities are responsible for the additional pressure gradient along the interface, consequently changing the interface topology, as discussed previously (Bojarevics and Pericleous, 2006). In addition to this, there is a significant effect from the bottom friction coefficient on the intensity of the horizontal circulation and the wave intensity. The value of Cf = 0.45 corresponds to the rough wall channel. This was used in most of the simulations. When changing this value to the smoother bottom situation, i.e., Cf = 0.045 (an order of magnitude less!), the cell becomes less stable, as can be seen from Figure 13. The horizontal circulation is also affected by the wave motion, and the oscillation can be felt in the turbulent horizontal velocities. This creates a modulation effect of the interface oscillations, as seen from Figure 13 when comparing the oscillations for the case with artificially made stationary horizontal circulation after the initial transient of 100 s.

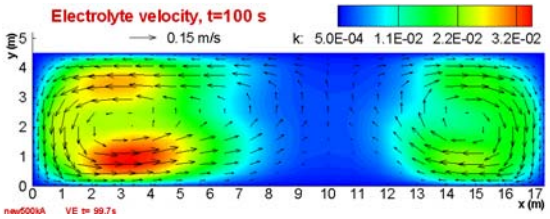


**Figure 11**: The horizontal velocity and the turbulent kinetic energy distribution in the liquid electrolyte.

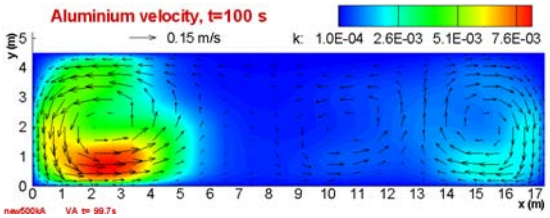


**Figure 12**: The horizontal velocity and the turbulent kinetic energy distribution in the liquid metal, t=100 s.

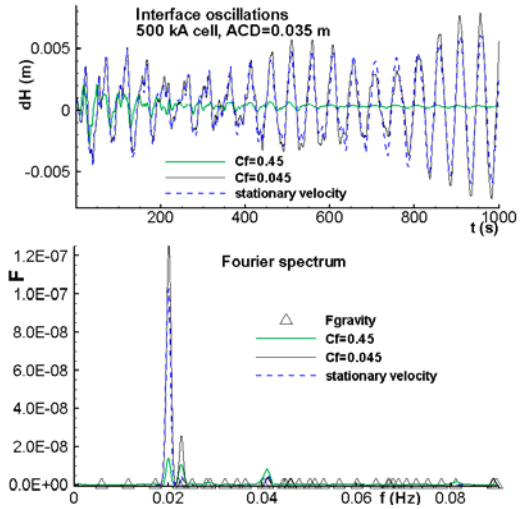


**Figure 13**: The oscillations (top) and the corresponding Fourier spectra (bottom) compared for different bottom friction coefficient values and the case when the horizontal circulation is kept stationary after initial 100 s.

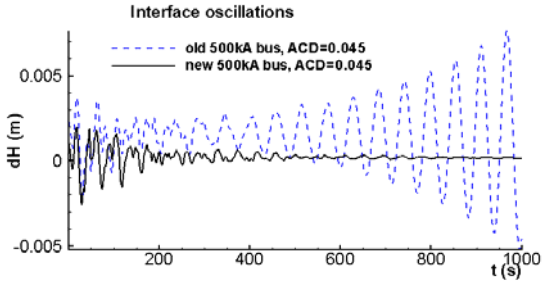


**Figure 14**: The liquid metal surface oscillations compared for the two bus arrangements.

Finally, we would like to note that the newly modified version of the 500 kA bus arrangement is significantly more stable than the one previously considered, as demonstrated in Figure 14. The previous bus design led to a stable cell only for the ACD increased to 0.055 m, whereas the new one is stable for 0.045 m ACD.

## CONCLUSION

The user friendly MHD numerical programme package simulates the real cell behaviour including the full coupling between the hydrodynamic and electrodynamic fields at all times. The inclusion of various design elements and physical factors are of importance for predicting the cell response to operation practice and the particular cell parameters.

## REFERENCES


VON KAENEL R. and ANTILLE J.P., (1996), "Magnetohydrodynamic stability in alumina reduction cells", *Travaux,* **23**, no. 27, 285-297.

URATA, N., MORI, K. and IKEUCHI, H., (1976), "Behavior of bath and molten metal in aluminium electrolytic cell", *Keikinzoku*, **26**, no. 11, 573-600.

SELE Th., (1977), "Instabilities of the metal surface in electrolytic alumina reduction cells", *Metallurgical Transactions B,* **8B**, 613-618.

SNEYD A. D. and WANG A., (1994), "Interfacial instability due to MHD mode coupling in aluminium reduction cells", *J. Fluid Mech.*, **263**, 343-359.

MOREAU R. and EWANS J.W., (1984), "An analysis of the hydrodynamics of aluminium reduction cells", *Journal of Electrochemical Society*, **131**, no. 10, 2251-2259.

RASTOGI A.K. and RODI W., (1978), "Prediction of heat and mass transfer in open channels", *J. Hydraulics Division ASCE,* **HY3,** 397-420.

BOJAREVICS V. and ROMERIO M. V. (1994), "Long waves instability of liquid metal-electrolyte interface in aluminium electrolysis cells: a generalization of Sele's criterion", *Eur. J. Mech., B/Fluids*, **13**, no 1, 33-56.

BOJAREVICS V., (1998), "Nonlinear waves with electromagnetic interaction in aluminium electrolysis cells", *Progr. Fluid Flow Res.: Turbulence and Applied MHD. AIAA*, Chapter 58, 833-848.

BOJAREVICS V. and PERICLEOUS K. (2006), "Comparison of MHD models for aluminium reduction cells", *Light Metals 2006*, (TMS), 347-352.